CTH analysis of Tantalum EFP formation using the BCJ model

R. A. Regueiro, M. F. Horstemeyer
Center for Materials and Engineering Sciences
Sandia National Laboratories
Livermore, CA 94551-0969, USA

Summary

This paper presents an Eulerian shock physics analysis of the formation of a Tantalum explosively-formed projectile (EFP). Recent modifications to the Bammann-Chiesa-Johnson (BCJ) thermo-visco-poro-plasticity model are briefly described. Specifically, a general pressure and porosity-dependent yield function is incorporated within the BCJ model in order to be able to consider various representations of porosity (a.k.a., damage) evolution. Experimental observation of an EFP event is compared with CTH simulations considering different representations of porosity evolution.

Introduction

The EFP is a munition design being studied by the armed services. An EFP results from a thin disk-shaped liner being loaded by an explosively-formed pressure wave from behind the liner. In this case the liner is Tantalum. An Eulerian shock physics code, such as Sandia's CTH, is especially well-suited to simulate impact events such as an EFP impacting a target (the eventual simulation of interest to the armed services). In order for the material response of the Tantalum liner to be appropriately modeled, a physically-based constitutive model like the BCJ model must be used. One concern in the past has been over-prediction of porosity evolution by the BCJ model. This paper focuses on this aspect of the BCJ model.

BCJ Model

The BCJ model captures the temperature and rate-dependent behavior of porous metals [1-4]. It assumes a multiplicative decomposition of the deformation gradient $\boldsymbol{F} = \boldsymbol{F}^e \boldsymbol{F}^p \boldsymbol{F}^v$ [2,3] (e for elastic, p for deviatoric plastic, and v for volumetric porosity), assumes small elastic deformation, a spatially random distribution of spherical voids (isotropic damage), uses a hardening-minus-recovery format for its internal state variables, and defines a form for the magnitude of the spatial plastic deformation rate $\|\boldsymbol{d}^p\|$ which leads to a unified creep plasticity model [12]. The thermodynamics of the BCJ model have been described in [2]. The pressure-dependent form of the BCJ model presented in this paper is adapted from [5]. In summary, the evolution equations for the pressure-dependent BCJ model are written in the current configuration as

$$\overset{\circ}{\boldsymbol{\sigma}} = (1-\phi)\,\boldsymbol{C} : (\boldsymbol{d} - \boldsymbol{d}^i) - \frac{\dot{\phi}}{1-\phi}\boldsymbol{\sigma} \tag{1}$$

$$\overset{\circ}{\boldsymbol{a}} = h(\theta)\|\boldsymbol{d}^i\|\boldsymbol{n}^a - \left[\sqrt{\frac{2}{3}} r_d(\theta)\|\boldsymbol{d}^i\| + r_s(\theta)\right]\sqrt{\frac{2}{3}}\|\boldsymbol{a}\|\boldsymbol{a} \tag{2}$$

$$\dot{\kappa} = \sqrt{\frac{2}{3}} H(\theta)\|\boldsymbol{d}^i\| - \left[\sqrt{\frac{2}{3}} R_d(\theta)\|\boldsymbol{d}^i\| + R_s(\theta)\right]\kappa^2 \tag{3}$$

$$\dot{\phi} = (1-\phi)\,\mathrm{tr}(\boldsymbol{d}^i) \tag{4}$$

$$\|\boldsymbol{d}^p\| \;=\; \sqrt{\frac{3}{2}} f(\theta) \sinh\left[\frac{\sqrt{\frac{3}{2}h_1\boldsymbol{\xi}:\boldsymbol{\xi} + h_2(\mathrm{tr}\boldsymbol{\Xi})^2} \;-\; h_3(\kappa + Y(\theta))}{h_3 V(\theta)}\right] \tag{5}$$

where $\boldsymbol{\sigma}$ is the Cauchy stress tensor, $\boldsymbol{a}$ is the backstress tensor internal state variable, κ is the scalar internal state variable, ϕ is the porosity internal state variable (defined as the volume of voids per unit total volume), θ is temperature, $\boldsymbol{C}$ is the constant fourth order elastic modulus tensor, $\boldsymbol{d}$ is the spatial deformation rate, $\boldsymbol{d}^i$ $(= \boldsymbol{d}^p + \boldsymbol{d}^v)$ is the spatial inelastic deformation rate, $\boldsymbol{d}^p$ is the spatial plastic deformation rate, $\boldsymbol{d}^v$ is the spatial isotropic porosity deformation rate, and $\boldsymbol{n}^a$ is the backstress direction tensor. The effective stresses are $\boldsymbol{\Xi} = \boldsymbol{\sigma} - (2/3)\boldsymbol{a}$ and $\boldsymbol{\xi} = \boldsymbol{\Xi} - \mathrm{tr}(\boldsymbol{\Xi})/3\,\mathbf{1}$. In this paper, $(\dot{})$ denotes material time derivative, and $(\circ)$ is an objective rate. The temperature-dependent yield and hardening-recovery functions are expressed in Arrhenius form as

$$\begin{aligned}
V(\theta) \;&=\; c_1 e^{-c_2/\theta}\;; \quad Y(\theta) \;=\; \frac{c_3}{c_{21} + e^{-c_4/\theta}} \frac{1}{2}\left[1 + \tanh(c_{19}(c_{20} - \theta))\right]\;; \quad f(\theta) \;=\; c_5 e^{-c_6/\theta} \\
r_d(\theta) \;&=\; c_7 e^{-c_8/\theta}\;; \quad h(\theta) \;=\; c_9 - c_{10}\theta\;; \quad r_s(\theta) \;=\; c_{11} e^{-c_{12}/\theta} \\
R_d(\theta) \;&=\; c_{13} e^{-c_{14}/\theta}\;; \quad H(\theta) \;=\; c_{15} - c_{16}\theta\;; \quad R_s(\theta) \;=\; c_{17} e^{-c_{18}/\theta}
\end{aligned} \tag{6}$$

where subscripts d and s denote dynamic and static recovery, respectively. In this paper, the porosity evolution equation through $\boldsymbol{d}^v$ will have two forms: (1) implicitly derived from the pressure-dependent yield function in elliptic form with parameters from [10], and (2) explicitly chosen based on the void growth evolution equation in [11]. The coefficients $h_i(\phi, m)$, $(i = 1, 2, 3)$ for the implicit form in (5) [10,5] are

$$h_1 \;=\; 1 + \frac{2}{3}\phi\,,\; h_2 \;=\; \frac{\phi}{2(1+m)(1+\phi)}\,,\; h_3 \;=\; (1-\phi)^{(1/(m+1))} \tag{7}$$

where m is the strain rate sensitivity parameter. The model is considered associative if the direction of inelastic deformation $\boldsymbol{n}^i = \boldsymbol{d}^i/\|\boldsymbol{d}^i\|$ is normal to the yield surface, i.e.

$$\boldsymbol{n}^i \;=\; \boldsymbol{n}^\sigma \;\Longrightarrow\; \text{associative}\;; \quad \boldsymbol{n}^\sigma \;:=\; \frac{\frac{\partial F}{\partial \boldsymbol{\sigma}}}{\left\|\frac{\partial F}{\partial \boldsymbol{\sigma}}\right\|}\,. \tag{8}$$

The rate-dependent yield function F is derived by inverting (5) to obtain

$$F \;=\; \sqrt{\frac{3}{2}h_1\boldsymbol{\xi}:\boldsymbol{\xi} + h_2(\mathrm{tr}\boldsymbol{\Xi})^2} \;-\; h_3\left(\kappa + Y(\theta) + V(\theta)\sinh^{-1}\left(\frac{\sqrt{\frac{2}{3}}\|\boldsymbol{d}^p\|}{f(\theta)}\right)\right)\,. \tag{9}$$

The numerical integration of the evolution equations (1-5) follows a standard radial return algorithm [9] within an explicit time integration of the governing equations (as in CTH [15]). This integration will be discussed in a future paper [16].

CTH analysis of Ta EFP formation

The BCJ constants were determined for commercially pure tantalum using the uniaxial compression experimental data provided in [7] and a fitting program described in [8]. The constants are given in Table 1 in units required by CTH (1.0eV converts to 11604.5K), and the resulting BCJ model

fits are shown in Figs. 1 and 2. The first set of BCJ constants in column 2 of Table 1 fit all the data well except the 77K data. The second set of BCJ constants in column 3 of Table 1 fit all the high strain rate data well and the low rate 77K (0.001/s) data reasonably well but do not fit the low rate 298K (0.1/s and 0.001/s) data well. The first set of BCJ constants in column 2 of Table 1 is used for the EFP simulations conducted with CTH. The rate sensitivity parameter m is taken from [13]. The spall strength p_0^f is taken from [14].

Three different forms of the BCJ model were used to simulate the EFP formation: (1) associative, pressure-dependent yield, void growth model from [10], (2) non-associative, pressure-dependent yield, void growth model from [11], and (3) associative, pressure-independent yield, void growth model from [11]. Two-dimensional axisymmetry was assumed. The three final shapes compared to the experimental EFP x-ray outline [6], as well as porosity contours, are shown in Fig. 3, where the three cases are shown in order from left to right. An initial porosity of $\phi_0 = 10^{-5}$ is assumed. Case (1) matches the observed outline best and does not predict significant porosity evolution (the clear contour represents porosity below 10^{-4}). For case (2), the end of the EFP has been punched out, and the dark gray contour represents approximately 0.4 porosity; the lighter gray contour represents porosity between 0.001 and

	no 77K	77K
ρ (g/cm^3)	16.6	16.6
E (dyne/cm^2)	1.68×10^{12}	1.68×10^{12}
ν	0.34	0.34
c_1 (dyne/cm^2)	4.5×10^{7}	5.0×10^{7}
c_2 (eV)	-0.04	0.0
c_3 (dyne/cm^2)	2.5×10^{7}	9.0×10^{8}
c_4 (eV)	0.078	0.086
c_5 (1/s)	4.0×10^{-6}	1.0×10^{-5}
c_6 (eV)	0.0	0.0
c_7 (cm^2/dyne)	4.0×10^{-9}	4.0×10^{-9}
c_8 (eV)	0.055	0.052
c_9 (dyne/cm^2)	5.23×10^{9}	1.7×10^{9}
c_{10} (dyne/(eV cm^2))	4.6×10^{8}	9.3×10^{8}
c_{11} (cm^2/(dyne s))	0.0	0.0
c_{12} (eV)	0.0	0.0
c_{13} (cm^2/dyne)	3.3×10^{-8}	1.6×10^{-8}
c_{14} (eV)	0.10	0.12
c_{15} (dyne/cm^2)	2.6×10^{10}	1.9×10^{10}
c_{16} (dyne/(eV cm^2))	1.2×10^{11}	4.6×10^{9}
c_{17} (cm^2/(dyne s))	5.0×10^{-6}	9.0×10^{-7}
c_{18} (eV)	4.0×10^{-4}	-0.06
c_{19} (1/eV)	0.0	11.6
c_{20} (eV)	0.0	0.02
c_{21}	0.0	0.06
m	4.2	4.2
p_0^f (dyne/cm^2)	6.23×10^{10}	6.23×10^{10}

Table 1. BCJ constants for Tantalum.

0.1. For case (3), the light gray contour is 0.99 porosity (maximum value of ϕ allowed in CTH), and clearly the EFP has completely failed, which is a shortcoming of the void growth model in [11] when used in conjunction with a pressure-independent yield function. Since these results only provide a qualitative comparison of the three different porosity evolution representations, further study is needed in order to determine a physically-based model of porosity evolution occurring in tantalum EFP's. For quantitative prediction of EFP formation, three-dimensional CTH simulations are required.

Conclusion

This paper briefly presented modifications to the damage part of the BCJ model. Three different representations of porosity evolution were used to simulate a Ta EFP formation, which led to significantly different EFP shapes and porosity contours. Further study is needed to determine the most physically-based pressure and porosity dependent yield function and porosity evolution equation for modeling damage in metals. Models of void nucleation and coalescence, besides void growth, are also being investigated [17].

Acknowledgement

Sandia is a multiprogram laboratory operated by Sandia Corporation, a Lockheed Martin Company, for the United States Department of Energy under contract DE-ACO4-94AL85000.

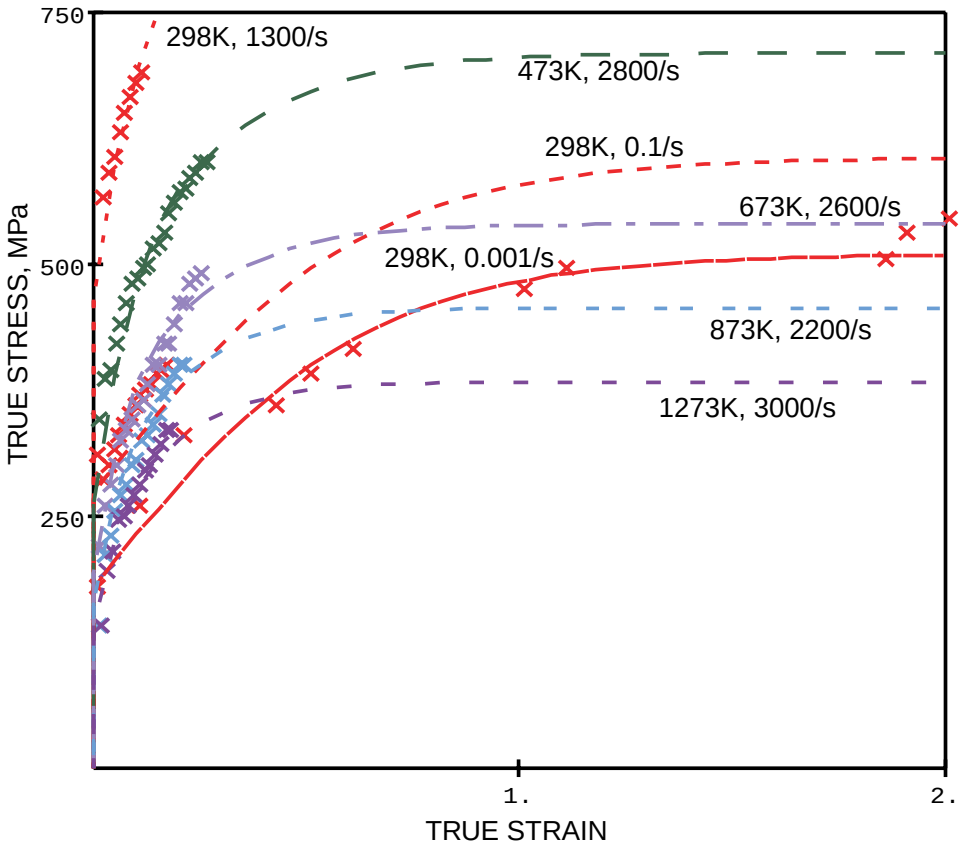

Figure 1. BCJ model (solid and dashed lines) and experimental data ("X" points) from [7] without 77K data, up to 200% strain.

References

1. Bammann, D.J. and Aifantis, E.C. (1989): "A damage model for ductile metals", *Nuclear Engineering and Design*, Vol. 116, pp. 355–362.
2. Bammann, D.J., Chiesa, M.L. and Johnson, G.C. (1996): "Modeling large deformation and failure in manufacturing processes", *Theoretical and Applied Mechanics*, Tatsumi, T., Watanabe, E. and Kambe, T. (Eds.), Elsevier, pp. 359–376.
3. Bammann, D.J. and Aifantis, E.C. (1987): "A model for finite-deformation plasticity", *Acta Mechanica*, Vol. 69, pp. 97–117.
4. Bammann, D.J., Chiesa, M.L., Horstemeyer, M.F. and Weingarten, L.I. (1993): "Failure in ductile materials using finite element methods", *Structural Crashworthiness and Failure*, Jones, N. and Wierzbicki, T. (Eds.), Elsevier, pp. 1–54.
5. Marin, E.B. and McDowell, D.L. (1996): "Associative versus non-associative porous viscoplasticity based on internal state variable concepts", *International Journal of Plasticity*, Vol. 12, No. 5, pp. 629–669.
6. Baker, E.L., Vuong, T. and Fuchs, B. (1996): "EFP and shaped charge concrete penetration", *7th TARDEC Ground Vehicle Survivability Symposium*, Monterey, CA.
7. Chen, S.R. and Gray, G.T., III (1996): "Constitutive behavior of Tantalum and Tantalum-Tungsten alloys", *Metallurgical and Materials Transactions A*, Vol. 27A, pp. 2994–3006.
8. Lathrop, J.F. (1996): "BFIT–A program to analyze and fit the BCJ model parameters to experimental Data–Tutorial and user's guide", Sandia National Laboratories, Report 97-8218.

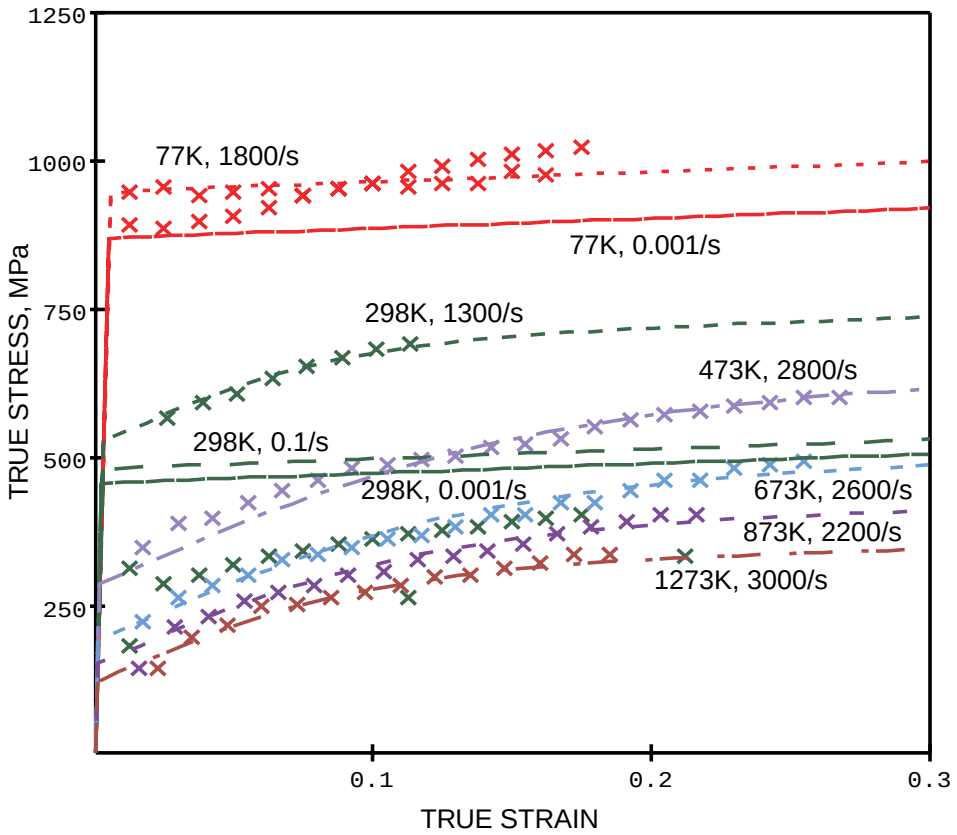

Figure 2. BCJ model (solid and dashed lines) and experimental data ("X" points) from [7] with 77K data, up to 30% strain.

9. Krieg, R.D. and Key, S.W. (1976): "Implementation of a time independent plasticity theory into structural computer programs", *Constitutive Equations in Viscoplasticity*, Stricklin, J.A. and Saczalski, K.J. (Eds.), pp. 125–137.
10. Cocks, A.C.F. (1989): "Inelastic deformation of porous materials", *Journal of the Mechanics and Physics of Solids*, Vol. 37, No. 6, pp. 693–715.
11. Cocks, A.C.F. and Ashby, M.F. (1980): "Intergranular fracture during power-law creep under multiaxial stresses", *Metal Science*, pp. 395–402.
12. Miller, A.K. (Ed.) (1987): *Unified Constitutive Equations for Creep and Plasticity*, Elsevier.
13. Frost, H.J. and Ashby, M.F. (1982): *Deformation-Mechanism Maps*, Pergamon Press.
14. Chhabildas, L.C., Barker, L.M., Asay, J.R., Trucano, T.G., Schmidt, S.C., Johnson, J.N. and Davison, L.W. (1989): "Spall strength measurements on shock-loaded refractory metals", *Shock Compression of Condensed Matter*, North Holland, pp. 429–432.
15. Taylor, P.A. (1996): "CTH Reference Manual: The Bammann-Chiesa-Johnson Viscoplastic/Damage Model", Sandia National Laboratories, Report 96-1626.
16. Regueiro, R.A. (2000): "Numerical implementation of a pressure and porosity-dependent yield function for a thermo-visco-poro-plasticity model in an Eulerian shock physics code", in preparation.
17. Horstemeyer, M.F. and Gokhale, A.M. (1999): "A void-crack nucleation model for ductile metals", *International Journal of Solids and Structures*, Vol. 36, No. 33, pp. 5029–5055.

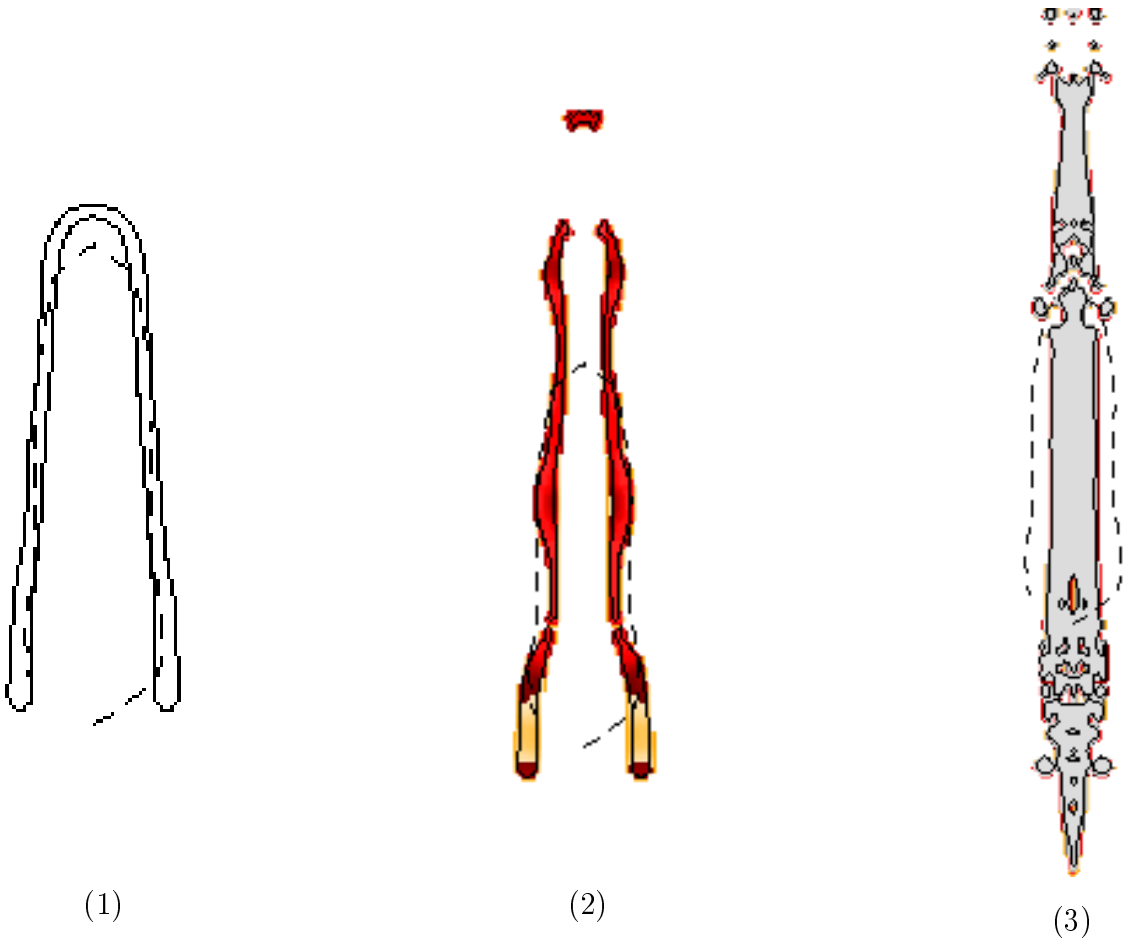

Figure 3. Comparison of different BCJ damage models for EFP formation at 400 μs. Dashed line is x-ray image outline of EFP [6].